Geochimica et Cosmochimica Acta, Vol. 68, No. 23, pp. 4905–4914, 2004

0016-7037/04 $30.00 + .00

ELSEVIER

doi:10.1016/j.gca.2004.05.033

Magnetite solubility and iron transport in magmatic-hydrothermal environments

ADAM C. SIMON,[1,*†] THOMAS PETTKE,[2] PHILIP A. CANDELA,[1] PHILIP M. PICCOLI,[1] and CHRISTOPH A. HEINRICH[2]

[1]Laboratory for Mineral Deposits Research, Department of Geology, University of Maryland, College Park, MD 20742, USA
[2]Isotope Geochemistry and Mineral Resources, Federal Institute of Technology, ETH Zentrum NO, CH-8092 Zurich, Switzerland

(*Received December* 3, 2003; *accepted in revised form May* 11, 2004)

Abstract—We have examined the effect of pressure on the apparent equilibrium constant, K′, for magnetite solubility ($Fe_3O_4^{mt} + 6HCl^{fluid} + H_2^{fluid} = 3FeCl_2^{fluid} + 4H_2O^{fluid}$) and the relative iron-carrying capacities of magmatic vapor and brine by conducting experiments in a rhyolite melt-vapor-brine-magnetite system at 800°C, f_{O_2} = NNO and pressures ranging from 100 to 145 MPa. Iron concentrations in synthetic vapor and brine fluid inclusions were quantified by using laser-ablation inductively-coupled-plasma-mass-spectrometry (LA-ICPMS). Hydrogen chloride (HCl) concentrations in magmatic vapor were inferred by potentiometric measurements of H^+ in quenched run product fluids. These data yield calculated values for log K′, assuming $a_{H_2O} = X_{H_2O}$, of 1.7, 4.9, 6.2, 6.8 and 9.1 at 100, 110, 130, 140 and 145 MPa, respectively. The concentration of iron in magmatic vapor increases by an order of magnitude, whereas the concentration of iron in magmatic brine remains constant (within 1σ) with increasing pressure as the 800°C critical pressure is approached along the vapor-brine solvus. The concentrations of iron in vapor and brine fluid inclusions yield calculated partition coefficients ($D_{Fe}^{v/b}$) of 0.05, 0.14, 0.27 and 0.56 at 110, 130, 140 and 145 MPa, respectively. Our data reveal that pressure fluctuations may significantly affect the value of log K′. More importantly, the data demonstrate conclusively that a significant amount of iron can be transported by a low-density aqueous vapor in the magmatic-hydrothermal environment.

1. INTRODUCTION

Magnetite is a nearly ubiquitous accessory mineral in a wide variety of igneous and metamorphic rocks and an important primary and secondary constituent of many magmatic-hydrothermal ore deposits. In intermediate to felsic igneous rocks genetically associated with porphyry-type ore deposits, magnetite can account for a significant proportion of the whole-rock iron content. Fluid inclusion data from natural magmatic-hydrothermal systems indicate that iron is one of the most abundant solute constituents of high-temperature magmatic-hydrothermal fluids evolved from shallow-level felsic magmas (Touret, 1971; Roedder, 1972; Poty et al., 1974; Roedder, 1984; Heinrich et al., 1992; Audétat et al., 1998, 2000), consistent with a link between felsic magmas and some large-scale magnetite- and iron sulfide-bearing ore deposits (Eugster and Chou, 1979; Sillitoe, 1993; Clark and Arancibia, 1995). This field relationship has prompted interest in quantifying the solubility of magnetite in magmatic fluids and their ability to deliver iron from magmas to the overlying country rock (Stirnemann, 1925; Ralston, 1929; Emmett and Schultz, 1933; Krauskopf, 1957; Holser and Schneer, 1961; Chou and Eugster, 1977; Boctor et al., 1980; Frantz et al., 1980; Whitney et al., 1985).

Experimental data for magnetite solubility indicate that iron is transported as $FeCl_2^0$ in sulfur-free, chloride-bearing supercritical fluids (Chou and Eugster, 1977; Boctor et al., 1980; Frantz et al., 1980). These studies report hat magnetite solubility is a function of the HCl concentration of the supercritical fluid and the hydrogen fugacity of the system. Chou and Eugster (1977) proposed that magnetite solubility is controlled by the equilibrium

$$Fe_3O_4^{mt} + 6\,HCl^{fluid} + H_2^{fluid} = 3\,FeCl_2^{fluid} + 4\,H_2O^{fluid} \quad (1)$$

where mt stands for magnetite and fluid stands for a one-phase magmatic hydrothermal fluid. It should be noted that the term fluid encompasses all single phase aqueous solutions of variable salinity and density. No activity coefficient data for solute species were available and, thus, values were reported for the apparent equilibrium constant, K′, for magnetite solubility determined at temperatures of 500 to 650°C and 200 MPa as

$$K'_{P,T} = \frac{(m_{FeCl_2}^{fluid})^3 (X_{H_2O}^{fluid})^4}{(a_{Fe_3O_4}^{mt})(m_{HCl}^{fluid})^6 (f_{H_2})} \quad (2)$$

where m stands for molality, X stands for mole fraction of H_2O in the supercritical fluid, a stands for activity, and f_{H_2} stands for fugacity of hydrogen. Boctor et al. (1980) performed experiments on hematite solubility in supercritical fluids and confirmed that iron is present dominantly as ferrous-chloride at oxygen fugacities close to the hematite-magnetite solid-state oxygen fugacity buffer between 400 and 600°C at 100 and 200 MPa. Frantz et al. (1980) reduced these datasets and published equations of the form

$$\log K'(P) = A + \frac{B}{T(\mathrm{K})} \quad (3)$$

where A and B are constants at 100 and 200 MPa and K is kelvins. This equation and the published constants, A and B of −25.218 and 30,361.8 at 100 MPa and −16.835 and 25,124.1 at 200 MPa, can be used to calculate apparent equilibrium constants within the range of experimental conditions.

Quantifying the HCl concentration of trapped magmatic flu-

* Author to whom correspondence should be addressed (asimon@jhu.edu).
† *Present address:* Department of Earth and Planetary Sciences, Johns Hopkins University, Baltimore, MD 21218 USA

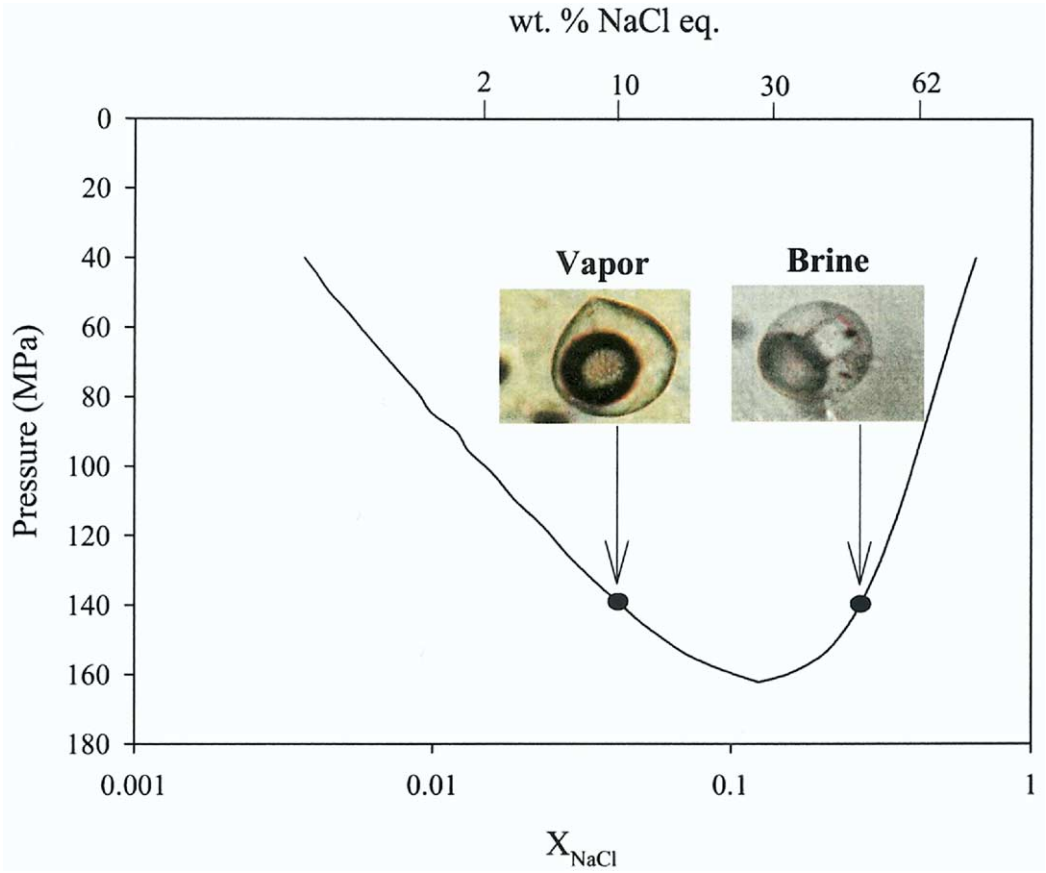

Fig. 1. Isothermal section of the system NaCl-H_2O at 800°C (modeled after Anderko and Pitzer, 1993). X_{NaCl} = mole fraction of NaCl in the pure NaCl-H_2O system. The curve outlines the miscibility gap as a function of pressure at 800°C; within this gap vapor and brine coexist as two immiscible and physico-chemically distinct magmatic volatile phases. The inset photomicrographs of vapor (liquid + vapor at ambient conditions) and brine (liquid + vapor bubble + halite at ambient conditions) are from an experiment at 140 MPa and 800°C. wt.% NaCl eq. values are presented along the upper abscissa.

ids is fundamental to understanding its effect on the reactivity of such fluids as well as impacting the solubility of ore metals such as Au (Frank et al., 2002) and Cu (Williams et al., 1995). The measured concentration of iron in natural fluid inclusions can serve as an indicator of the HCl concentration of the trapped fluid (Eqn. 1) if we assume appropriate values for oxygen fugacity, activity of magnetite, pressure and temperature. Candela and Piccoli (1995) used a combination of Eqn. 2 and 3 to calculate the concentration of $FeCl_2$ in magmatic vapor exsolved from melt during isobaric, isothermal second boiling (i.e., volatile exsolution owing to the crystallization of anhydrous minerals from the melt phase) at 100 MPa and 800°C. The temperature used in the model of Candela and Piccoli (1995) is two hundred degrees higher than the highest experiment of Frantz et al. (1980) used to derive their equation for magnetite solubility. Candela and Piccoli (1995) used these equations because they provided the only means by which $FeCl_2$ could be calculated in the magmatic volatile phase. However, the extrapolation of these equations to the supersolidus conditions at which two fluids, a vapor and a brine, coexist and that is encountered during the early evolutionary stages of many high-temperature magmatic-hydrothermal systems may not accurately predict solute iron concentrations.

Fluid inclusion evidence from natural systems indicates that the aqueous fluid exsolved from a crystallizing melt in either the one-phase or two-phase field can be can be approximated by the NaCl-H_2O binary system (Roedder, 1984; Bodnar et al., 1985). Examination of the pressure-volume-temperature-composition (*PVTX*) phase relations in the NaCl-H_2O system (Fig. 1) indicates that at the prevailing range of pressures and temperatures associated with magmatic intrusions in Earth's shallow crust, a water-chloride fluid may commonly separate into coexisting vapor and brine (Sourirajan and Kennedy, 1962; Henley and McNabb, 1978; Bodnar et al., 1985; Chou, 1987; Fournier, 1987). Whereas both vapor and brine can rise buoyantly in the magma, the lower-density vapor phase will pass more easily through the magma column owing to greater buoyancy and lower viscosity of the vapor (Hedenquist, 1995). Note however, that subtle changes in pressure, for a given temperature, can cause large variations in the equilibrium concentration of NaCl in coexisting aqueous vapor and brine (Fig. 1). For example, at 800°C and 100 MPa the wt.% concentrations of NaCl of vapor and brine are ~2 and 60, respectively, while at 800°C and 145 MPa they are 20 (vapor) and 35 (brine). This systematic variation in vapor and brine salinity as a function of pressure may have important implications for magnetite solu-

Table 1. Composition of synthetic rhyolite.

Oxide	wt.%
SiO_2	75.18
Al_2O_3	11.09
K_2O	4.43
Na_2O	3.67
CaO	0.17
Fe_2O_3	0.04
MnO	0.01
MgO	0.10
TiO_2	0.03
P_2O_5	0.03
LOI	4.51
Total	99.26

Chemical composition of the starting glass used in all experiments as determined by XRF (Frank, 2001).
LOI = loss on ignition.

bility and the concentration of iron (and other solutes) in magmatic vapors and brines owing to an expected positive relationship between increasing pressure and the concentration of HCl in vapors and brines (Williams et al., 1997).

Based on the NaCl-H_2O *PVTX* systematics at a given temperature, the pressure at which a melt undergoes volatile exsolution should significantly affect the iron-carrying capacity of the fluids. This is relevant to the magmatic-hydrothermal environment wherein melts commonly undergo volatile exsolution across a depth range of several kilometers, corresponding to lithostatic pressures between ~50 and ~150 MPa (e.g., Audétat and Pettke, 2003). Within this pressure range the solidus temperature for wet granite ranges from ~650°C to ~700 (Tuttle and Bowen, 1958; Luth et al., 1964; von Platten, 1965; Piwinskii, 1968; Merrill et al., 1970; Robertson and Wyllie, 1971). However, magmatic fluid exsolution and, therefore, the scavenging of iron by this fluid start at super-solidus temperatures as a result of decreasing lithostatic pressure (defined as first boiling) and/or second boiling. The goal of the present experimental study is to quantify the partitioning of iron between haplogranite melt and a free volatile phase and, as such, we performed all experiments at 800°C to eliminate the crystallization of silicate phases during runs and to expedite equilibration between all phase components of the experimental charge. Future experiments will be performed at temperatures closer to the haplogranite solidus to assess the effect of temperature on magnetite solubility and iron partitioning. The 800°C vapor-brine solvus in the NaCl-H_2O system, a proxy for more complex magmatically-generated fluids, indicate that at all pressures below ~160 MPa a vesiculating melt with an initial value of Cl/H_2O equal to 0.05 by weight will exsolve coexisting chloride-bearing vapor and brine (Anderko and Pitzer, 1993; Candela and Piccoli, 1995). A melt with an initial weight ratio of $Cl/H_2O \leq 0.05$ will exsolve only a low-density aqueous fluid, and the concentration of chloride in the melt and coexisting vapor will increase until brine saturation. For a given f_{H2}^{sys}, a_{Fe3O4}^{mt}, and f_{H2O}^{v}, the HCl concentration of the low-density magmatic vapor controls the solubility of magnetite (Chou and Eugster, 1977). Quantifying the relationship between pressure, magnetite solubility and the concentration of iron in the fluids will allow a more accurate prediction of the concentration of iron in high-temperature fluids, conditions relevant for the ore-forming magmatic-hydrothermal environment.

Here we report experimentally-determined apparent equilibrium constants for magnetite solubility in magmatic vapor that are broadly consistent, albeit higher than values of log K′ calculated with the equations of Frantz et al. (1980) based on the extrapolation of extant data from the one-phase fluid field at lower temperature. We also report data that quantify the concentration of iron in coexisting vapors and brines at several pressures corresponding to an approximate lithostatic depth interval of 4 to 6 km beneath Earth's surface. These data elucidate the effect of pressure on the relative abilities of magmatic vapor and brine to scavenge and transport iron within the magmatic-hydrothermal environment.

2. PROCEDURES

2.1. Experimental Procedures

Experiments were performed near, but just outside, the 800°C vapor solvus of the model NaCl-H_2O system at pressures of 100, 110, 130, 140 and 145 MPa in a magnetite–rhyolite melt–vapor–brine–gold metal capsule assemblage. The gold capsules were loaded with 40 mg magnetite (Cornwall, Pennsylvania), 40 mg synthetic rhyolite, a fractured Brazilian quartz chip and 100 μL aqueous solution containing dissolved NaCl, KCl and HCl. The chemical composition of the rhyolite is provided in Table 1. The molar ratio of Na:K:H was set to unity in all starting aqueous solutions. The chemical composition of the starting fluids is provided in Table 2. The starting magnetite:melt:fluid mass ratio was 1:1:2.5 in all experiments. EPMA data indicated that magnetite was nearly end-member Fe_3O_4 ($a_{Fe3O4}^{mt} \approx 1$). A rhyolite melt was included because we also aimed to investigate potential melt-vapor-brine exchange relationships between iron, sodium and po-

Table 2. Composition of starting aqueous solutions.

P (MPa)	Number of runs	Initial wt.% NaCl eq.	NaCl (μg/g) (± 2σ)	KCl (μg/g) (± 2σ)	HCl (μg/g) (± 2σ)
100	3	1.8	6000 ± 120	7653 ± 134	3741 ± 72
110	3	2.5	10,005 ± 210	12,764 ± 255	6242 ± 125
130	4	5	18,331 ± 366	23,391 ± 465	11,436 ± 230
140	2	10	33,356 ± 667	42,523 ± 850	20,789 ± 410
145	3	20	66,667 ± 1300	85,047 ± 1700	41,578 ± 825

Experimental solutions were prepared by adding reagent grade solid salts of NaCl and KCl and concentrated aqueous HCl (11.66 molar) to doubly deionized, distilled water. The reported uncertainty reflects error in the measured mass (NaCl and KCl) and volume (HCl) of salts added to the starting solutions.

Table 3. LA-ICPMS data for coexisting vapor and brine fluid inclusions and AAS data for quenched fluids.

P (MPa)	Number of runs	Type of inclusions analyzed	Number of inclusions analyzed	Bulk[a] wt.% NaCl eq.	Final[b] wt.% NaCl eq.	HCl[c] (μg/g) ($\pm 2\sigma$)	Na (μg/g) ($\pm 2\sigma$)	K (μg/g) ($\pm 2\sigma$)	Fe (μg/g) ($\pm 2\sigma$)
100[d]	3	NA[e]	NA[e]	1.8	1.4–1.7	2700 ± 350	2200 ± 210	2100 ± 270	1900 ± 110
110[f]	4	See below	NA[f]	2.5	2.1–2.4	970 ± 110	6400 ± 520	6000 ± 780	3100 ± 350
110	3	Vapor	17	2.5	2.1–2.4	970 ± 110	5500 ± 840	5800 ± 800	3100 ± 740
110	3	Brine	12	2.5	56–58	NR[g]	140,000 ± 8000	150,000 ± 16,000	64,000 ± 6000
130	4	Vapor	13	5.5	4.9–5.3	1000 ± 260	9500 ± 2200	14,000 ± 2000	10,000 ± 2600
130	4	Brine	6	5.5	50–53	NR[g]	110,000 ± 10,000	130,000 ± 20,000	72,000 ± 20,000
140	2	Vapor	8	10	8.8–9.3	1100 ± 230	17,000 ± 6900	27,000 ± 6000	20,000 ± 2000
140	2	Brine	6	10	42–44	NR[g]	82,000 ± 6000	110,000 ± 10,000	73,000 ± 18,000
145	3	Vapor	10	20	18.7–19.2	670 ± 90	32,000 ± 8700	66,000 ± 30,000	41,000 ± 7700
145	3	Brine	8	20	35–37	NR[g]	59,000 ± 18,000	120,000 ± 40,000	72,000 ± 16,000

[a] Bulk wt.% NaCl eq. indicates the salinity of the starting aqueous solution.
[b] Final salinities are the range of wt.% NaCl eq. values for synthetic vapor and brine fluid inclusions as determined by microthermometry.
[c] HCl concentrations calculated from potentiometrically determined hydrogen ion concentrations in quenched fluids.
[d] Data for runs at 100 MPa were measured by AAS.
[e] No fluid inclusions were deemed suitable for analysis in these runs.
[f] Concentrations in this row were measured by AAS and are reported to allow comparison with LA-ICPMS data.
[g] The reported HCl concentrations for vapor represent the HCl concentration of the quenched experimental fluid which consisted of >95% vapor by mass. Owing to the strong partitioning of HCl into vapor coexisting with brine (Williams et al., 1997) we feel that the measured HCl concentrations approximate the HCl concentration of the experimental vapor.

tassium as well as to elucidate the behavior of gold in a melt-magnetite-vapor-brine assemblage; these data will be presented in separate publications.

The gold capsules (4.8-mm ID, 5-mm OD, 30-mm length) were placed inside cold-seal René-41 pressure vessels pressurized by water as the pressure medium and heated in solid, doubly-wound, tube furnaces. Charges were loaded with 40 mg magnetite, 40 mg synthetic rhyolite, a prefractured quartz chip and 100 μL aqueous solution. The loaded capsules were immersed in dry ice and welded shut. Sealed capsules were placed in a drying oven (110°C) for 4 h, and maintenance of capsule mass (±3 mg) was used to verify the integrity of welded capsules. Charges were pressurized to ~50 MPa, heated to 800°C and then pressurized to the final run pressure. Temperatures were measured with type K (Chromel-Alumel) external thermocouples that were calibrated against internal thermocouples in the presence of the water-pressure medium for each experimental vessel. The temperature gradient in each experimental vessel was minimized by maintaining the hot end of the vessel and the furnace at a 10° angle from horizontal (following Charles and Vidale, 1982). The maximum temperature uncertainty at all pressures was ± 5°C over the 3 cm long capsule, as determined by internal calibration in the presence of the water-pressure medium. The combination of a low temperature gradient and tilted vessel position minimizes the potential for thermally-induced convection gradients and this, in turn, retards premature healing of the prefractured quartz chips. This lack of premature healing is critical to the experimental goal of trapping aqueous fluids that have equilibrated with all the phase components of the charge. Pressure was imposed by an air-driven water-pressure intensifier and monitored with Bourdon-tube gauges (±2 MPa) calibrated against a factory-calibrated Heise gauge. The use of René-41 vessels, a Ni-based alloy, and the water pressure medium imposed an oxygen fugacity equal to the nickel-nickel oxide (NNO) solid-state oxygen fugacity buffer on the experimental charge as verified in our laboratory using the Ag-AgCl sensor technique (Frank, 2001). Experiments were quenched isobarically along a two-stage cooling path involving air stream cooling from 800 to 200°C followed by immersion in an ambient-temperature water bath. Capsules were removed from the vessels, cleaned, examined microscopically and weighed to determine if the capsules remained sealed during the experiment. Only capsules that exhibited mechanical integrity were processed for analysis.

Coexisting vapor and brine were trapped as synthetic fluid inclusions in the prefractured quartz crystals, demonstrating that all experiments were vapor + brine saturated. The mass proportion of vapor to brine in all experiments is > 95:1, as determined by using the lever rule and the salinities of the initial aqueous solution and measured wt.% NaCl eq. values for the vapor and brine fluid inclusions. This suggests that the addition of KCl, HCl and $FeCl_2$ to the binary NaCl-H_2O system widens the miscibility gap at the experimental conditions.

2.2. Analytical Procedures

2.2.1. Analyses of Quenched Fluids

The top end of each recovered experimental capsule was pierced with a stainless steel hypodermic syringe, and the quenched aqueous solution was removed and transferred to a weighed volumetric flask. "Blanks" were prepared and analyzed by sampling prepared acidic solutions with the syringes. These trials indicated convincingly that the syringe did not contaminate recovered solutions. Recovered aqueous solutions were weighed and diluted for atomic absorption spectrophotometry (AAS) and potentiometric (pH) analyses. The HCl concentration of experimental fluids are provided in Table 3. An air-acetylene flame was used to quantify the concentrations of Na, K and Fe. Concentrations were determined by linear regression using a six point standard calibration curve within the linear working range for the analytical instrument as veri-

Table 4. EPMA analyses of major elements and chlorine in the run product glasses.

P (MPa)	SiO2 (wt.%) (± 2σ)	K_2O (wt.%) (± 2σ)	Na_2O (wt.%) (± 2σ)	FeO (wt.%) (± 2σ)	Al_2O_3 (wt.%) (± 2σ)	Cl (wt.%) (±2σ)	Total	ASI
100	74.01 ± 1.60	4.96 ± 0.36	3.54 ± 0.32	1.17 ± 0.70	10.64 ± 0.98	0.24 ± 0.10	94.56	0.95
110	73.06 ± 1.33	4.88 ± 0.29	4.43 ± 0.65	1.40 ± 0.37	10.92 ± 0.77	0.20 ± 0.04	94.89	0.87
130	72.65 ± 1.30	5.21 ± 0.28	4.30 ± 0.46	1.09 ± 0.30	10.97 ± 0.99	0.22 ± 0.05	94.44	0.86
140	73.54 ± 2.07	5.16 ± 0.35	3.77 ± 0.53	1.03 ± 0.29	10.43 ± 0.99	0.21 ± 0.06	94.14	0.89
145	72.72 ± 1.54	5.21 ± 0.26	3.34 ± 0.42	1.07 ± 0.28	9.78 ± 0.82	0.20 ± 0.03	92.32	0.88

Each datum represents the average of a minimum of 10 spot analyses in different areas of a given experimental glass. ASI was calculated as the molar ratio $[Al_2O_3/(Na_2O + K_2O)]$ The calculated values of ASI indicate that all experimental melts were peralkaline. Uncertainties are presented as twice the standard deviation from the mean ($\pm 2\sigma$) for the replicate measurements of each glass.

fied for each element in our laboratory. Table 3 lists the concentrations of Na, K and Fe in experimental solutions at 100 and 110 MPa. The AAS-determined concentrations of these cations in the higher pressure (i.e., 130, 140 and 145 MPa) solutions deviated from the LA-ICPMS data, most likely owing to precipitation of salts during quench, and, thus, the iron concentrations determined by LA-ICPMS were used to calculate apparent equilibrium constants at pressures of 110 MPa and higher.

The HCl concentration of the quenched experimental fluids was determined by measuring fluid pH using a Beckman φ40 pH meter equipped with an AccupHast electrode. To properly quantify the activity vs. concentration function for hydrogen ion in the quenched solutions we prepared pH standards with reagent grade HCl to define a pH range that overlapped the expected pH of the quenched solutions and we added reagent grade NaCl and KCl in proportions corresponding to the expected concentrations of these salts in the quenched experimental solutions. This procedure minimizes the error owing to matrix effects on the measured pH values. The determined M_{H^+} in the quenched fluid is assumed to represent the hydrogen ion concentration that was present as associated HCl in the experimental fluid as HCl completely dissociates during quench (Tagirov et al., 1997). While this assumption ignores the possibility of subsolidus reactions that can affect the M_{H^+}, all charges were analyzed within 1 to 2 h of quench and, thus, we feel that this assumption is justified. Table 3 lists the concentration of HCl in experimental solutions at 100, 110, 130, 140 and 145 MPa. It should be noted that the potentiometrically determined hydrogen concentrations represent the hydrogen in the quenched aqueous fluid, consisting of coexisting vapor and brine at run conditions. The calculated mass proportion of vapor:brine in all experiments was determined by using the lever rule and the data for salinity of the starting aqueous solution and the measured wt.% NaCl eq. values of vapor and brine fluid inclusions. The proportion of vapor:brine is $> 95{:}1$ by weight at all experimental conditions and, thus, we feel that the effects of fluid phase separation during the experiments are negligible for the calculation of the equilibrium constant for magnetite solubility in the fluid. Owing to the strong partitioning of HCl into vapor coexisting with brine (Williams et al., 1997) we infer the measured HCl concentrations to approximate the HCl concentration of the experimental vapor.

2.2.2. Analyses of Experimental Glasses

Quantitative characterization of silicate glass (i.e., quenched rhyolite melt) was performed by wavelength dispersive spectrometry (WDS) using a JEOL JXA 8900 electron microprobe. Samples were prepared for analysis by coating them with a ~0.03 μm carbon film using standard thermal evaporation techniques. Operating conditions for glass analyses were 15-keV accelerating potential, 5-nA beam current, and a 15-μm beam size with minimum counting times of 20 s (sum of peak and background). Glasses were analyzed at multiple locations to evaluate melt homogeneity. As pointed out by Morgan and London (1996) and Acosta-Vigil et al. (2003), sodium migration and concomitant aluminum and silicon burn-in during the analysis of hydrous aluminosilicate glasses can cause significant analytical bias. We performed multiple analyses to determine if these phenomena occurred and found no systematic problem in glasses with variable sodium and water concentrations. Yellowstone rhyolite (NMNH 72854 VG568) was used to standardize Si, Al, Na and K. Kakanui hornblende (USNM 143956) was used to standardize Fe. Scapolite (Meionite, Brazil, USNM R6600-1) was used to standardize Cl. EPMA data for the experimental glasses indicate that all experimental melts were mildly peralkaline (i.e., ASI = 0.86 to 0.95; ASI calculated as the molar ratio $[Al_2O_3/(Na_2O + K_2O)]$). The glass compositions are presented in Table 4.

2.2.3. Analyses of Synthetic Fluid Inclusions

Recovered chips of Brazilian quartz were agitated ultrasonically in doubly deionized and distilled H_2O for 30 min to remove surficial contaminants. The quartz chips were set in epoxy, sectioned longitudinally into wafers (~500 μm thick) and then polished on both sides for petrographic examination, microthermometry and LA-ICPMS analysis.

Salinities of vapor and brine inclusions were determined by freezing point depression (i.e., Tm_{ice}) and final dissolution of halite (i.e., Td_{NaCl}), respectively. Microthermometric measurements were performed using a USGS-type gas flow heating-freezing stage manufactured by Fluid, Inc. The thermocouple was placed directly on the sample to hold the sample and to reduce the uncertainty in temperature measurements. Apparent salinities for magmatic vapors and brines expressed as NaCl equivalent (wt.% NaCl eq.) were calculated using the equations of Bodnar and Vityk (1994) and are reported in Table 3.

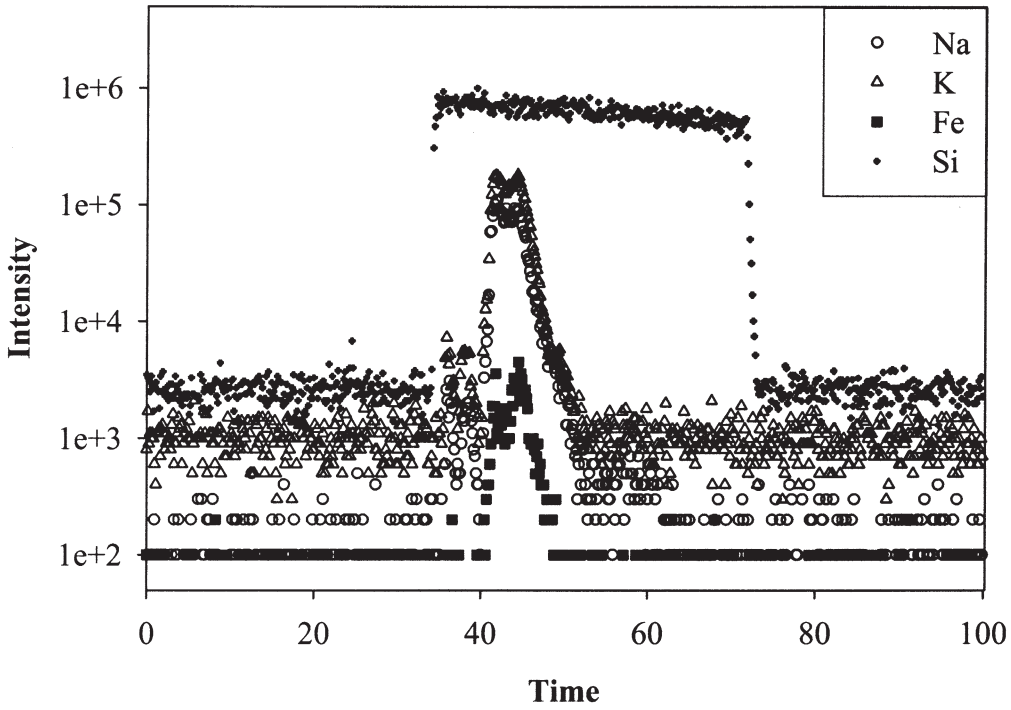

Fig. 2. LA-ICPMS transient signal a vapor fluid inclusion (~23 μm across; ~20 μm deep; 19 wt.% NaCl eq.) hosted within quartz. A 30-μm beam diameter was used to ablate the entire inclusion. Ablation of quartz began at ~35 s and the fluid inclusion was liberated from ~40 to 53 s.

The solute concentrations of synthetic vapor and brine inclusions were quantified individually by LA-ICPMS using an energy-homogenized (Microlas), pulsed 193-nm ArF Excimer laser (Compex 110i, Lamda Physik) that enables controlled ablation (Günther et al., 1998; Heinrich et al., 2003). Laser ablation was performed in a 1-cm^3 ablation chamber and monitored with a video camera that permitted constant observation of the sample surface during ablation. The diameter of the laser beam was set slightly larger than the maximum dimension of the fluid inclusions such that the entire inclusion was ablated together with a minimal volume of surrounding matrix quartz.

A representative LA-ICPMS transient signal of a vapor inclusion (~23; 19 wt.% NaCl eq.) from a depth of ~20 μm is shown in Figure 2. The signal consists of gas background (0–34 and 73–100 s), quartz (34–40 and 49–73 s) and quartz plus vapor fluid inclusion (40–49 s). The transient signal for each analysis was integrated, and element ratios (e.g., Fe:Na) were quantified using a National Institute of Standards and Technology (NIST) SRM 610 silicate glass. Element ratios determined by LA-ICPMS were transformed into absolute element concentrations using sodium as the internal standard. Absolute concentrations of sodium in each fluid inclusion were determined by correcting the wt.% NaCl eq., determined by microthermometry for the presence of KCl and $FeCl_2$ via the equation $NaCl_{true} = NaCl_{equiv} - 0.5 \times \Sigma X^n{+}Cl_n$ which assumes that all major cations in the fluid inclusion were present as chloride salts (Heinrich et al., 2003). Note that element ratios, and hence partition coefficients, are independent of this assumption. Table 3 lists the concentrations of Na, K and Fe in synthetic fluid inclusions as quantified by LA-ICPMS. Data for synthetic fluid inclusions from experiments at 100 MPa were not collected owing to a dearth of suitable inclusions for analysis.

2.3. Demonstration of Equilibrium

The success of any experimental study is predicated on the ability to achieve equilibrium and, thus, here we present a discussion of the attainment of equilibrium in experimental vapors and brines before entrapment as fluid inclusions in quartz chips. Experiments were performed for times ranging from 150 to 597 h. These experimental timescales are consistent with previous experimental studies that demonstrated equilibrium in H_2O-saturated peralkaline assemblages (Carmichael and Mackenzie, 1963; Thompson and Mackenzie, 1967; Bailey et al., 1974; Bailey and Cooper, 1978; Scaillet and MacDonald, 2001). The goal of our experimental design was to produce equilibrated magmatic fluids that would migrate into preexisting fractures in a quartz chip before the quartz underwent self-healing. To inhibit premature self-healing of quartz microfractures we minimized the thermal gradient along the length of the charge and, furthermore, we titled the vessel to retard thermal convection. The thermal gradient was ±5°C over the 3-cm-long capsule (i.e., 3.3°C cm^{-1}). The rods of quartz were cut to ~1 cm in length and the rod is positioned toward the low end of the capsule (i.e., the capsule is titled 10° from horizontal). Thus, the temperature along the quartz rod inside the capsule did not vary by more than 3°C. Despite this experimental configuration to retard self-healing of quartz microfractures, we do not know the kinetics of healing quartz fractures at the current experimental conditions. Brantley (1992) reported that quartz microfractures, in the presence of NaCl-H_2O fluids at 200 MPa and 600°C, undergo self-healing of ~50% of the length of a given fracture on a timescale of 5 h. Brantley's (1992) study indicates that many of the synthetic fluid inclu-

sions produced in our experiments will contain quickly trapped fluids which had not fully equilibrated with all phase components of the charge. To avoid analyzing prematurely formed fluid inclusions we selected individual fluid inclusions that had ice-melting and homogenization temperatures close to those predicted by the calculations of Bodnar and Vityk (1994) for the experimental conditions employed. While this does not guarantee that the fluid in each analyzed fluid inclusion represents an equilibrium solute load, we can use data from a separate experimental study, at conditions nearly identical to those in our study, involving the analysis of experimentally-produced fluid inclusions in glass to evaluate directly the potential for the fluids to have equilibrated before entrapment.

Frank et al. (2002) performed experiments in a rhyolite melt-brine-gold metal capsule assemblage at 800°C, 100 MPa and f_{O_2} = NNO and quantified the concentration of gold in fluid inclusions trapped in glass (i.e., quenched melt) using neutron activation (INAA). These fluid inclusions in glass trapped fluids that were in equilibrium with the charge until the moment the experiment was terminated. The composition of the rhyolite melt and the acidity of the magmatic fluid in the experiments of Frank et al. (2002) are identical to that used in our experiments. Frank et al. (2002) reported gold concentrations of 36 ± 4 mg/kg for experiments wherein the fluid had a concentration of HCl < 1000 mg/kg. Our experimentally produced fluid inclusions trapped in quartz microfractures, in a charge with a^{sys}_{Au}, contain gold concentrations of 35 ± 5 mg/kg at 800°C, f_{O_2} = NNO and a slightly higher pressure, 110 MPa, and similar low HCl conditions. We interpret this correspondence in gold concentrations between fluid inclusions trapped in melt and quartz as strong evidence that our selected fluid inclusions trapped in quartz microfractures contained equilibrated fluids. Our LA-ICPMS data for gold concentrations in coexisting vapor and brine will be presented in a separate publication.

3. RESULTS

3.1. Magnetite Solubility as a Function of Pressure

3.1.1. Iron Speciation in Experimental Fluids

Iron-speciation in magmatic volatile phases will be a function of the acidity, density and chlorine concentration of the aqueous fluid. To calculate apparent equilibrium constants using Eqn. 2 (Chou and Eugster, 1977), we assume that the dominant iron-species in our experimental solutions is $FeCl^0_2$. The presence of significant quantities of other iron-species, such as iron-hydroxide, would render use of Eqn. 2 invalid for our experimental conditions. The experimental fluids in Chou and Eugster (1977) had total chlorine concentrations that varied from 1.2 to 19.7 wt.%, largely overlapping those of our experiments (1.4–11.5 wt.%). The pressures of the earlier study also overlap those of the current study. The main difference between the two studies is the lower temperature range of the previous study, 500 to 650°C vs. 800°C in our case. Whereas this temperature contrast will certainly affect the density of the fluids, we treat the data assuming that the neutral iron-species, $FeCl^0_2$, is dominant.

Table 5. Calculated values of log K' for magnetite solubility.

P (MPa)	log $K'_{P,T}$
100	1.7 ± 0.7
110	4.9 ± 0.9
130	6.2 ± 2.5
140	6.8 ± 1.8
145	9.1 ± 1.2

All values of K' were calculated using the HCl concentration calculated from the potentiometrically determined hydrogen ion concentration in quenched fluid. The value for K' at 100 MPa was calculated using the iron concentration in the quenched fluid as measured by AAS. All other values of K' were calculated using iron concentrations obtained by LA-ICPMS. Uncertainties were calculated by propagating the error in iron, HCl and X_{H_2O} through Eqn. 2 using the general error propagation formula.

3.1.2. Determination of the Apparent Equilibrium Constant

Values for the apparent equilibrium constant for magnetite solubility, K′, were calculated by using Eqn. 2, and are listed in Table 5. The reported value of log K′ at 100 MPa was calculated using Fe and HCl concentrations of the quenched aqueous solution. The reported values of log K′ at 110, 130, 140 and 145 MPa were calculated using the HCl concentration in the quenched aqueous solution and the Fe concentrations in synthetic vapor fluid inclusions.

Apparent equilibrium constants were calculated by using our experimentally determined concentrations of Fe and HCl, and f_{H_2} was calculated by using equations of Huebner and Sato (1970) and Belonoshko et al. (1992). Magnetite was treated as a pure solid phase with $a^{mt}_{Fe_3O4}$ = 1. We assumed Raoultian behavior (i.e., $a^{v}_{H_2O} = X^{v}_{H_2O}$) for water and calculated values for $X^{v}_{H_2O}$ from mass balance of the quenched fluid at 100 MPa and from vapor fluid inclusions at all other pressures. Figure 3 shows the comparison between the new values for log K′ and those predicted using the equations from Frantz et al. (1980). For example, at 800°C, 100 MPa, f_{O_2} = NNO and a given m_{HCl} and X_{H_2O}, the calculated iron concentrations are 1900 and 5300 mg/kg using the new experimentally determined K′ and the equation of Frantz et al. (1980), respectively.

The experimental values for magnetite solubility, determined in this study, can be used to calculate model HCl concentrations of high-temperature, paleo-magmatic vapors and brines that had equilibrated with magnetite and were subsequently trapped as fluid inclusions in minerals that grew during an ore-forming event (Roedder and Bodnar, 1997). Once the concentration of iron in the fluid inclusion has been determined, if we assume appropriate values for oxygen fugacity, activity of magnetite, mole fraction of water, pressure and temperature, then calculating the model HCl concentration of the fluid responsible for the scavenging, transport and deposition of ore metals in magmatic-hydrothermal systems can be performed by rearranging the equation for the apparent equilibrium constant, K′ (Eqn. 2) as

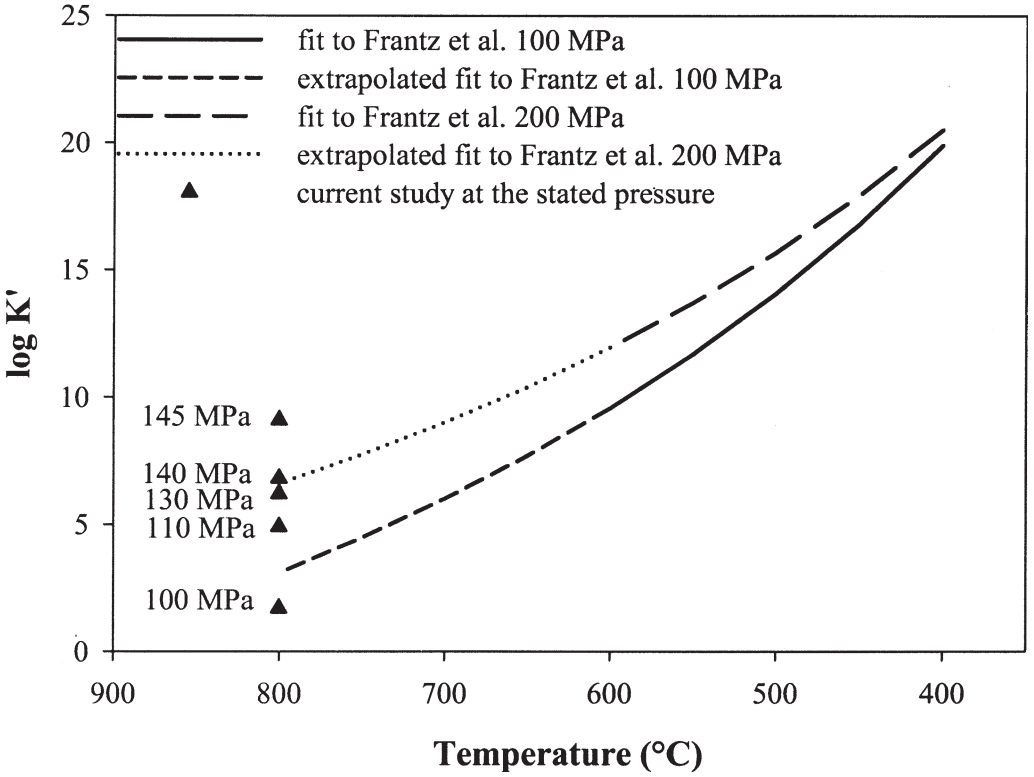

Fig. 3. Values for magnetite solubility calculated as apparent equilibrium constants as determined in the present study compared to those calculated using the equations of Frantz et al. (1980). The equations of Frantz et al. (1980) are fits to published experimental data collected at 400 to 600°C and, thus, the extension of lines beyond 600°C represent extrapolated values of log K′ based on their equations.

$$m^{v}_{HCl} = \left(\frac{(m^{fluid}_{FeCl_2})^3 \times (X^{fluid}_{H_2O})^4}{K' \times (a^{mt}_{Fe_3O_4}) \times (f_{H_2})} \right)^{\frac{1}{6}} \quad (4)$$

This is an important parameter for evaluating the ore-forming potential of magmatic systems, and also for estimating HCl inputs to the deep levels of geothermal systems.

3.2. Iron Segregation Between Vapor and Brine

3.2.1. Partitioning of Iron Between Vapor and Brine

Iron concentrations in brine-saturated magmatic vapor increase by an order of magnitude as the critical pressure is approached along the vapor limb of the 800°C solvus (Table 3). Iron is transported as $FeCl_2$ in the vapor phase and, thus, the correlation between iron and chloride was expected. In contrast to this behavior in the vapor, the iron concentration in the brine remains constant, within the analytical uncertainty, as the critical pressure is approached along the brine solvus (Table 3). Thus, as the chloride concentrations of vapor and brine converge along the solvus toward the critical pressure, increasing chloride concentration of the vapor has a strong positive effect on iron concentration whereas the analytical uncertainty does allow us to infer quantitatively the relationship between chloride and iron in brine. The iron concentrations of coexisting vapor and brine in our experiments yield calculated partition coefficients for iron between vapor and brine, $D^{v/b}_{Fe}$, as a function of pressure (Table 6). Figure 4 shows a strong positive correlation between $D^{v/b}_{Fe}$ and pressure; indicating that in a given melt-vapor-brine system the partitioning of iron between vapor and brine is a strong function of pressure.

4. CONCLUSIONS

We have experimentally quantified the equilibrium constant for magnetite solubility, K′, at 800°C, f^{sys}_{O2} = NNO and pressures between 100 and 145 MPa in a rhyolite melt-magnetite-

Table 6. Partition coefficient for iron between vapor and brine.

P (MPa)	$D_{Fe}{}^{v/b}$
110	0.05 ± 0.01
130	0.14 ± 0.04
140	0.27 ± 0.04
145	0.56 ± 0.01

Vapor-brine partition coefficients for iron as a of function pressure. All experiments were conducted at 800°C with NaCl-KCl-$FeCl_2$-HCl-bearing aqueous solutions. The critical pressure in the model NaCl-H_2O system is ~160 MPa at 800°C (Anderko and Pitzer, 1993). The uncertainties ($\pm 1\sigma$) were calculated by propagating the error in iron concentrations in vapor and brine fluid inclusions through the partition coefficient using the general error propagation formula.

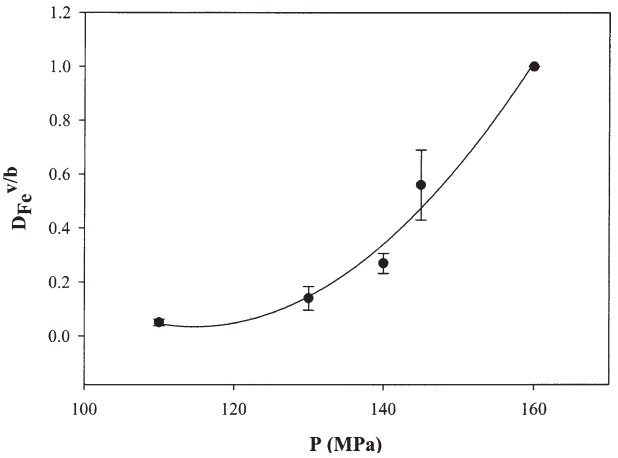

Fig. 4. Partition coefficient for iron between coexisting vapor and brine as a function of pressure. The datum at 160 MPa and $D_{Fe}^{v/b} = 1$ is constrained by the fact that at the critical pressure, ~160 MPa (Anderko and Pitzer, 1993), the vapor and brine phases become indistinguishable and with an incremental increase in pressure the vapor and brine become a single supercritical fluid. Error bars are $\pm 1\sigma$. The error in pressure determinations is on the order of 2 MPa and falls within the symbols. The curve is a second order polynomial fit to the experimental data and the constraint that $D_{Fe}^{v/b} = 1$ at the critical pressure.

vapor-brine assemblage. Our data demonstrate that the apparent equilibrium constant for magnetite solubility in subcritical, chloride-bearing vapors coexisting with brine at super-solidus temperatures varies significantly with pressure. We suggest that our data are valid for low-density single-phase aqueous fluids in general. Therefore, these values facilitate direct calculation of model HCl concentrations in magmatic vapors preserved as fluid inclusions in hydrothermal-magmatic systems and, thus, enable a more accurate understanding of the evolving chemistry of high-pressure vapors associated with magmatic-hydrothermal systems.

Concentrations of iron in synthetic vapor and brine fluid inclusions, trapped in quartz at 800°C, f_{O2}^{sys} = NNO and pressures between 110 and 145 MPa, were quantified by LA-ICPMS. The concentration of iron increases by an order of magnitude with increasing pressure whereas the concentrations of iron in brine does not vary outside the one sigma uncertainty with increasing pressure. The calculated partition coefficients for iron between coexisting vapor and brine increase systematically as pressure increases from 110 to 145 MPa. Our data demonstrate that volatile exsolution at pressures approaching the critical pressure enhances significantly the iron-carrying capacity of magmatic vapor and that ascending high-pressure vapor can deposit considerable quantities of magnetite. Over the integrated lifetime of a magmatic-hydrothermal system, high-pressure vapor has the capacity to deliver significant quantities of iron to the superjacent hydrothermal environment.

Acknowledgments—This work was partially supported by National Science Foundation (EAR 9909576 [PAC and PMP]; EAR 0125805 [PAC and PMP]; EAR 9810244 [PMP]), a Cosmos Club Foundation Student Research Grant and University of Maryland Graduate School Ilene H. Nagel Research Grant to ACS. We thank Mark Frank for providing experimental assistance in the early stages of this project. The Fluid and Ore Deposits Group at ETH acknowledges continued support for LA-ICPMS analytical development by the Swiss National Science Foundation. We also thank Liane Benning, Dave Vanko, Anthony Williams-Jones and an anonymous reviewer for their insightful comments. ACS also expresses thanks to Alicia, Abigail and James for providing support and plenty of needed diversions during the writing of this paper.

Associate editor: L. G. Benning

REFERENCES

Acosta-Vigil A., London D., Morgan G. B., and Dewers T. A. VI (2003) Solubility of excess alumina in hydrous granitic melts in equilibrium with peraluminous minerals at 700–800 C and 200 MPa and applications of the aluminum saturation index. *Contrib. Mineral. Petrol.* **146,** 100–119.

Anderko A. and Pitzer K. S. (1993) Equation-of-state representation of phase equilibria and volumetric properties of the system NaCl-H_2O above 573 K. *Geochim. Cosmochim. Acta* **57,** 1657–1680.

Audétat A. and Pettke T. (2003) The magmatic-hydrothermal evolution of two barren granites: A melt and fluid inclusion study of the Rito del Medio and Cañada Pinabete plutons in northern New Mexico (USA). *Geochim. Cosmochim. Acta* **67,** 97–121.

Audétat A., Günther D., and Heinrich C. A. (1998) Formation of a magmatic hydrothermal ore deposit; insights with LA-ICP-MS analysis of fluid inclusions. *Science* **279,** 2091–2094.

Audétat A., Günther D., and Heinrich C. A. (2000) Causes for large-scale metal zonation around mineralized plutons; fluid inclusion LA-ICP-MS evidence from the Mole Granite, Australia. *Econ. Geol.* **95,** 1563–1581.

Bailey D. K, and Cooper J. P. (1978) Comparison of the crystallization of pantelleritic obsidian under hydrous and anhydrous conditions. In *Progress in Experimental Petrology; Fourth Progress Report of Research Supported by N.E.R.C., 1975–1978* (ed. W. S. MacKenzie), pp. 230–233.

Bailey D. K., Cooper J. P., and Knight J. L. (1974) Anhydrous melting and crystallization of peralkaline obsidians. *Bull. Volcan.* **38,** 653–665.

Belonoshko A. B., Shi P. F., and Saxena S. K. (1992) A FORTRAN-77 program for calculation of Gibbs free energy and volume of C-H-O-S-N-Ar mixtures. *Comp. Geosci.* **18,** 1267–1269.

Boctor N. Z., Popp R. K., and Frantz J. D. (1980) Mineral-solution equilibria-IV. Solubilities and the thermodynamic properties of $Fe_2O_3^0$ in the system Fe_2O_3-H_2-H_2O-HCl. *Geochim. Cosmochim. Acta* **44,** 1509–1518.

Bodnar R. J. and Vityk M. O. (1994) Interpretation of microthermometric data for H2O NaCl fluid inclusions. In *Fluid Inclusions in Minerals, Methods and Applications* (eds. B. De Vivo and M. L. Frezzotti), pp. 117–130. Virginia Polytechnic Institute.

Bodnar R. J., Burnham C. W., and Sterner S. M. (1985) Synthetic fluid inclusions in natural quartz. III. Determination of phase equilibrium properties in the system H_2O-NaCl to 1000C and 1500 bars. *Geochim. Cosmochim. Acta* **49,** 1861–1873.

Brantley S. L. (1992) The effect of fluid chemistry on quartz microcrack lifetimes. *Earth Planet. Sci. Lett.* **113,** 145–56.

Candela P. A., Piccoli P. M. (1995) Model ore-metal partitioning from melts into vapor and vapor/brine mixtures. In *Magmas, Fluids and Ore Deposits* (ed. J. F. H. Thompson), **23**, pp. 101–128. Mineralogical Association of Canada.

Carmichael I. S. E. and MacKenzie W. S. (1963) Feldspar-liquid equilibria in pantellerites: An experimental study. *Am. J. Sci.* **261,** 382–396.

Charles R. W. and Vidale R. (1982) Temperature calibration of a new rapid quench vessel. *Am. Mineral.* **67,** 175–179.

Chou I. C. (1987) Phase relations in the system NaCl-KCl-H_2O: III, solubilities of halite in vapor-saturated liquids above 445 degrees C and redetermination of phase equilibrium properties in the system NaCl-H_2O to 1000 degrees C and 1500 bars. *Geochim. Cosmochim. Acta* **51,** 1965–1975.

Chou I. C. and Eugster H. P. (1977) Solubility of magnetite in supercritical chloride solutions. *Am. J. Sci.* **277,** 1296–1314.

Clark A. H. and Arancibia O. N. (1995) The occurrence, paragenesis and implications of magnetite-rich alteration-mineralization in

calc-alkaline porphyry copper deposits. In *Proceedings of the Second Giant Ore Deposits Workshop* (ed. A. H. Clark), pp. 511–581. Kingston, Canada, April 25–27.

Emmett P. H. and Schultz J. F. (1933) Equilibria in the system Fe-Fe_3O_4-H_2O-H_2 at 400, 500 and 600 C. *Am. Chem. Soc. J.* **55,** 1376–1389.

Eugster H. P. and Chou I. M. (1979) A model for the deposition of Cornwall-type magnetite deposits. *Econ. Geol.* **74,** 763–774.

Fournier R. O. (1987) Conceptual models of brine evolution in magmatic-hydrothermal systems. *U. S. Geol. Surv. Prof. Paper* **1350,** 1487–1506.

Frank M. (2001) *An Experimental Investigation of Ore Metals in Silicate Melt-Volatile Phase Systems*. Ph.D. dissertation, University of Maryland.

Frank M. R., Candela P. A., Piccoli P. M., and Glascock M. D. (2002) Gold solubility, speciation and partitioning as a function of HCl in the brine-silicate melt-metallic gold system at 800°C and 100 MPa. *Geochim. Cosmochim. Acta* **66,** 3719–3732.

Frantz J. D., Popp R. K., and Boctor N. Z. (1980) Solubility constants of rock-forming minerals. In *Carnegie Institution of Washington Year Book* **79,** 340–345.

Günther D., Audetat A., Frischknecht A., and Heinrich C. (1998) A quantitative analysis of major, minor and trace elements in fluid inclusions using laser ablation-inductively coupled plasma mass spectrometry. *J. Anal. Atom. Spectrom.* **13,** 263–270.

Hedenquist J. W. (1995) The ascent of magmatic fluid: Discharge versus mineralization. In *Magmas, Fluids and Ore Deposits* (ed. J. F. H. Thompson), **23,** pp. 263–289. Mineralogical Association of Canada.

Heinrich C. A., Ryan C. G., Mernagh T. P., and Eadington P. J. (1992) Segregation of ore metals between magmatic brine and vapor. *Econ. Geol.* **87,** 1566–1583.

Heinrich C. A., Pettke T., Halter W. E., Aigner-Torres M., Audétat A., Günther D., Hattendorf D., Bleiner D., Guillong M., and Horn I. (2003) Quantitative multi-element analysis of minerals, fluid and melt inclusions by laser-ablation inductively-coupled-plasma mass spectrometry. *Geochim. Cosmochim. Acta* **67,** 3473–3497.

Henley R. W. and McNabb A. (1978) Magmatic vapor plumes and ground-water interaction in porphyry copper emplacement. *Econ. Geol.* **73,** 1–20.

Holser W. T. and Schneer C. J. (1961) Hydrothermal magnetite, *Geol. Soc. Am. Bull.* **72,** 369–386.

Huebner J. S. and Sato M. S. (1970) The oxygen fugacity-temperature relationships of manganese oxide and nickel oxide buffers. *Am. Mineral.* **55,** 934–938.

Krauskopf K. B. (1957) The heavy metal content of magmatic vapor at 600 degrees C. *Econ. Geol.* **52,** 786–807.

Luth W. C., Jahns R. H., and Tuttle O. F. (1964) The granite system at pressure of 4 to 10 kilobars. *J. Geophys. Res.* **69,** 759–773.

Merrill R. J., Robertson J. K., and Wyllie P. J. (1970) Melting reactions in the system $NaAlSi_3O_8$-$KAlSi_3O_8$-SiO_2-H_2O to 20 kilobars compared with results for other feldspar-quartz-H2O and rock-H_2O systems. *J. Geol.* **78,** 558–569.

Morgan G. B.VI, and London D. (1996) Optimizing the electron microprobe analysis of hydrous alkali aluminosilicate glasses. *Am. Mineral.* **81,** 1176–1185.

Piwinskii A. J. (1968) Experimental studies of igneous rock series: Central Sierra Nevada batholith, California. *J. Geol.* **76,** 548–570.

Poty B., Stalder H. A., and Weisbrod A. (1974) Fluid inclusion studies in quartz from fissures of Western and Central Alps, *Schweiz. Mineral. Petrogr. Mittel.* **54,** 717–752.

Ralston O. C. (1929) Iron oxide reduction equilibria. *United States Bureau of Mines Bulletin* **296**.

Robertson J. K. and Wyllie P. J. (1971) Rock-water systems with special reference to the water deficient region. *Am. J. Sci.* **271,** 252–277.

Roedder E. (1972) Compositions of fluid inclusions. *U.S. Geol. Surv. Prof. Paper* **440**.

Roedder E. (1984) *Fluid Inclusions*. Mineralogical Society of America.

Roedder E. and Bodnar R. J. (1997) Fluid inclusion studies of hydrothermal ore deposits. In *Geochemistry of Hydrothermal Ore Deposits* (eds. T. M. Seward and H. L. Barnes), pp. 657–698. John Wiley, New York.

Scaillet B. and MacDonald R. (2001) Phase relations of peralkaline silicic magmas and petrogenetic implications. *J. Petrol.* **42,** 825–845.

Sillitoe R. H. (1993) Gold-rich porphyry copper deposits; geological model and exploration implications. In *Mineral Deposit Modeling* **40,** 403–417. Geological Society of Canada.

Sourirajan S. and Kennedy G. C. (1962) The system NaCl-H2O at elevated temperatures and pressures. *Am. J. Sci.* **260,** 115–141.

Stirnemann E. (1925) Das system eisenchlorid-wasser bei höherer temperatur. *Neues Jahr. Miner. Petr. Beil. B* **52A**, 334–377.

Tagirov B. R., Zoo A. V., and Kingie N. N. (1997) Experimental study of dissociation of HCl from 350 to 500C and from 500 to 2500 bars: Thermodynamic properties of HCl, *Geochim. Cosmochim. Acta* **61,** 4267–4280.

Thompson R. N. and MacKenzie W. S. (1967) Feldspar-liquid equilibria in peralkaline acid liquids: An experimental study. *Am. J. Sci.* **265,** 714–734.

Touret J. (1971) The granulite facies in Southern Norway: The fluid inclusions. *Lithos* **4,** 423–436.

Tuttle O. F. Bowen N. L. (1958) Origin of granite in the light of experimental studies in the system $NaAlSi_3O_8$-$KAlSi_3O_8$-SiO_2-H_2O. Geological Society of America Memograph 74.

von Platten H. (1965) Experimental anatexis and genesis of migmatites. In *Controls of Metamorphism* (eds. W. S. Pitcher and G. W. Flinn), pp. 203–218. John Wiley, New York.

Whitney J. A., Hemley J. J., and Simon F. O. (1985) The concentration of iron in chloride solutions equilibrated with synthetic granitic compositions; the sulfur free system. *Econ. Geol.* **80,** 444–460.

Williams T. J., Candela P. A., and Piccoli P. M. (1995) The partitioning of copper between silicate melts and two-phase aqueous fluids: An experimental investigation at kbar, 800°C and 0.5 kbar, 850°C. *Contrib. Miner. Petrol.* **121,** 388–399.

Williams T. J., Candela P. A., and Piccoli P. M. (1997) Hydrogen-alkali exchange between silicate melts and two-phase aqueous mixtures; an experimental investigation. *Contrib. Miner. Petrol.* **128,** 114–126.